Cell Reports, Volume *17*

Supplemental Information

Endophilin-A Deficiency Induces the Foxo3a-Fbxo32 Network in the Brain and Causes Dysregulation of Autophagy and the Ubiquitin-Proteasome System

John D. Murdoch, Christine M. Rostosky, Sindhuja Gowrisankaran, Amandeep S. Arora, Sandra-Fausia Soukup, Ramon Vidal, Vincenzo Capece, Siona Freytag, Andre Fischer, Patrik Verstreken, Stefan Bonn, Nuno Raimundo, and Ira Milosevic

Endophilin-A deficiency induces the FOXO3a-FBXO32 network in the brain and causes dysregulation of autophagy and the ubiquitin-proteasome system

John D. Murdoch[1,2]*, Christine M. Rostosky[1]*, Sindhuja Gowrisankaran[1], Amandeep S. Arora[1], Sandra F. Soukup[3,4], Ramon Vidal[5], Vincenzo Capece[5], Siona Freytag[1], Andre Fischer[6,7], Patrik Verstreken[3,4], Stefan Bonn[5], Nuno Raimundo[2]**, Ira Milosevic[1]**

Supplemental Figures and Figure legends

Figure S1, related to Figure 1

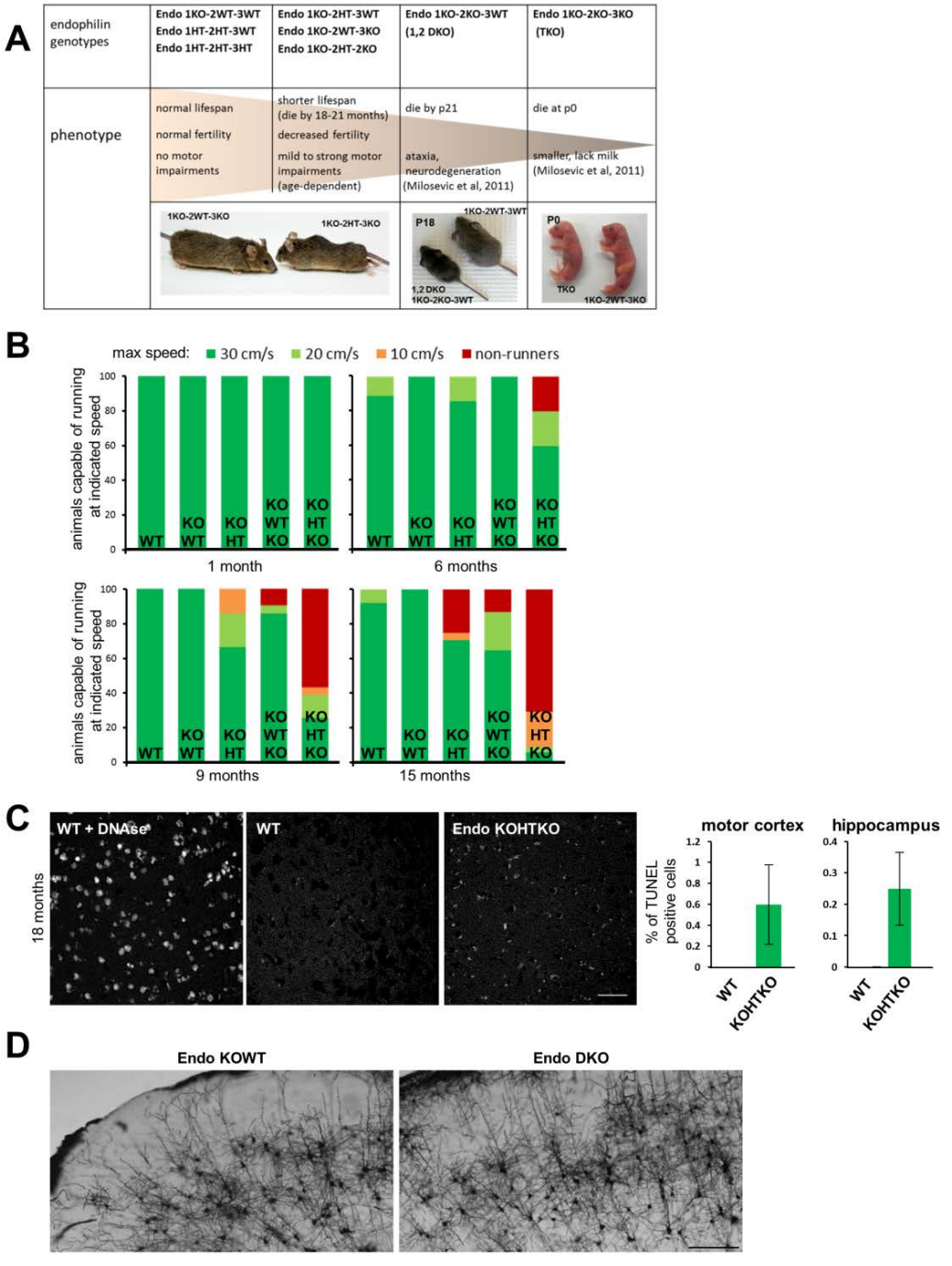

Figure S1. Motor impairments and neuronal cell death in mice with endophilin deficiency, related to Figure 1

(A) Schematic illustrating correlation between genotype and phenotype of endophilin mutant mice. Mammals have 3 endophilin-A genes (SH3GL2/endophilin-A1; SH3GL1/endophilin-A2; SH3GL3/endophilin-A3). Mice lacking endophilin-1 and 2 (1,2 DKO) and mice lacking all three endophilins (TKO) have impaired endocytosis and altered synaptic vesicle recycling. Endophilin TKO mice die 4-12 hours after birth, while endophilin 1,2 DKO live 2-3 weeks, show ataxia and mild to moderate neurodegeneration. Endophilin-1 single knock-out (KO) and heterozygous (1HT-2HT; 1HT-2HT-3HT) mice appear phenotypically normal and have normal lifespan, while endophilin 1KO-2HT and particularly 1KO-2HT-3KO mice exhibit shorter lifespans (~19 and ~18 months, respectively). Movie 1 and 2 show motor impairments in 1,2 DKO and 1KO-2HT-3KO mice that is independent from animal background (129Sv/J and 129Sv/J backcrossed to C56BL/6J).

(B) Highest speed that endophilin mutants were able to run on DigiGait at 1 (top-left), 6 (top-right), 9 (buttom-left) and 15 (buttom-right) months. Colors indicate percentage of mice able to run at 30 cm/s (green), 20 cm/s (light green), 10 cm/s (orange); red indicates animals refusing to run.

(C) Apoptosis in aged endophilin 1KO-2HT-3KO mice at 18 months: TUNEL assay was performed on brain sections of mice with indicated genotypes. DNAse treated WT sections were used as positive control for condensed DNA in the nucleus (shown by arrows) Scale bar 50µm. Right: Quantification of positive cells in motor cortex and hippocampus. Data are expressed as mean±SEM.

(D) Cortex of endophilin 1,2 DKO (p18) and littermate control by Golgi staining. Overall cell morphology is not altered. Scale bar: 200µm.

Figure S2, related to Figures 2 and 3

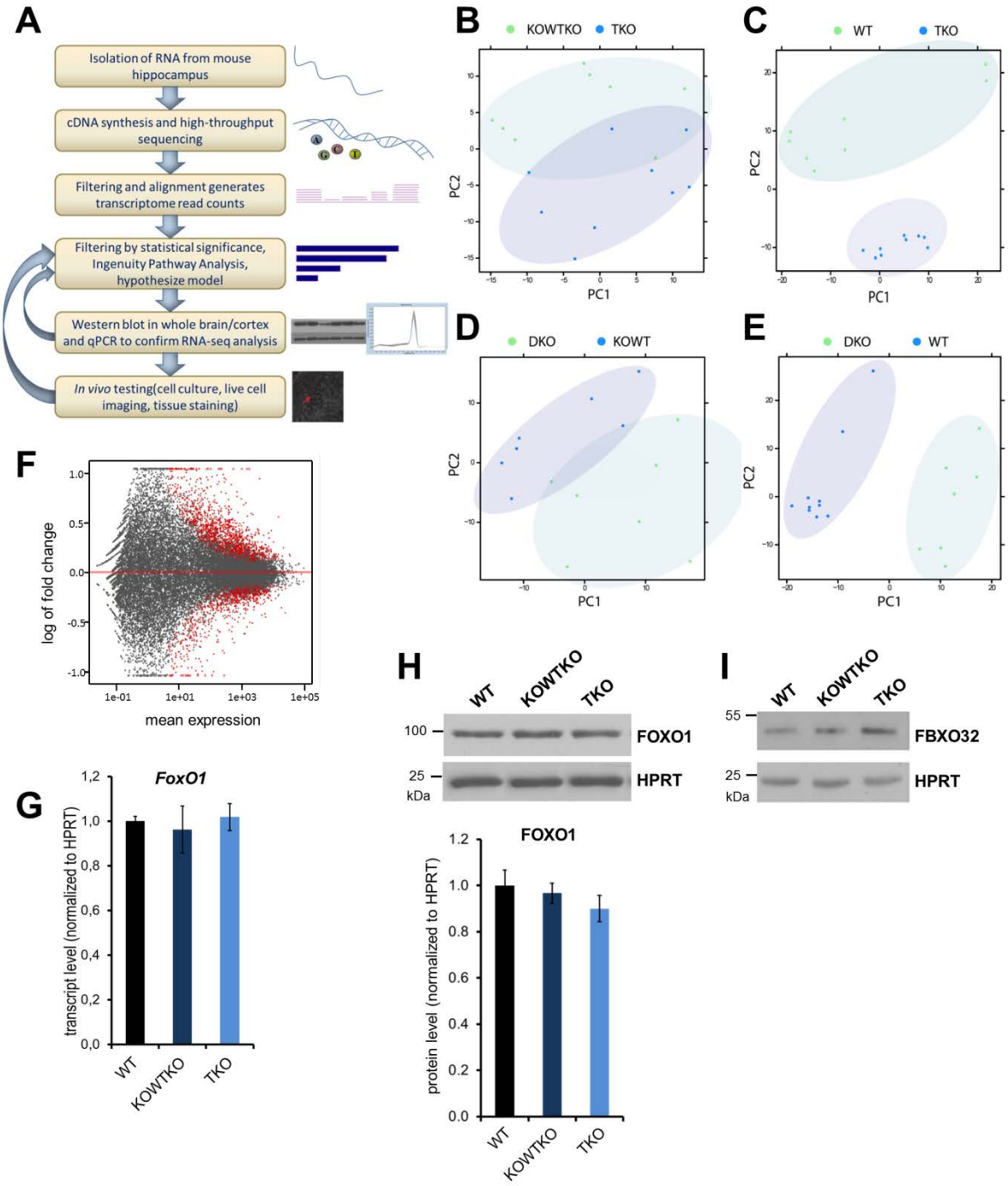

Figure S2. Integrative genomic analysis of endophilin TKO and 1,2 DKO hippocampi and verification experiments, related to Figures 2 and 3

(A) Experimental strategy highlighting the steps of RNA isolation from hippocampus, sequencing, mapping, statistical analysis and data verification.

(B) Endophilin TKO and littermate endophilin 1KO-2WT-3KO mice RNA-sequencing samples as assessed by principal component (PC) analysis. Data are present in Suppl Table 2.

(C) Endophilin TKO RNA-sequencing samples clearly segregated from WT samples by principal component analysis. Data are presented in Suppl Table 3.

(D) RNA-sequencing samples from endophilin 1,2 DKO and littermate endophilin 1KO-2WT mice as assessed by principal component analysis. Data are presented in Suppl Table 5.

(E) Endophilin 1,2 DKO RNA-sequencing samples clearly segregated from WT samples by principal component analysis. Data are presented in Suppl Table 6.

(F) RNA-sequencing of endophilin TKO vs. control (WT+littermates) hippocampi samples yield 2176 differentially expressed genes with nominal p-value<0.01. Data are presented in Suppl Table 7 and shown here in a volcano plot depicting the logarithmic fold change and the mean expression. Each dot represents one gene; the differentially expressed genes are depicted in red.

(G) Transcript levels of *Foxo1*, as measured by quantitative real-time PCR, in endophilin TKO samples and corresponding controls. $p>0.05$, Student's t test, error bars: SEM.

(H) Protein analysis by Western blotting revealed no change in FOXO1 levels in endophilin TKO whole brain extracts in comparison to corresponding controls. Below: Quantification of immunoblots for FOXO1 (normalized to the loading control). $p>0.05$, Student's t test, error bars: SEM.

(I) Representative Western blot showing upregulation of FBXO32 in endophilin TKO hippocampus (compared to WT and littermate control). The loading control (HPRT) is shown below.

Figure S3, related to Figures 3 and 4

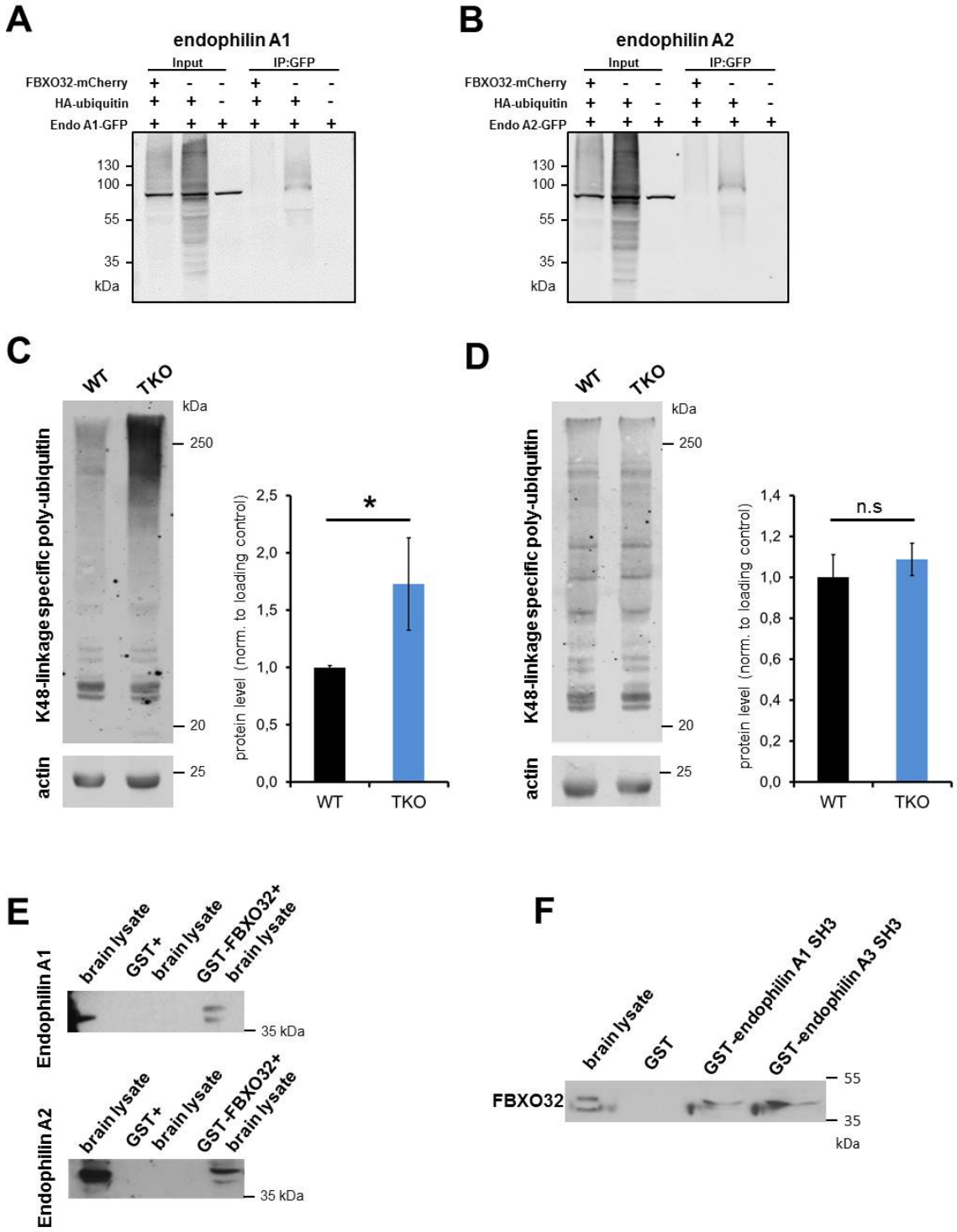

Figure S3. **FBXO32 does not ubiquitinate endophilin-1 and 2, related to Figures 3 and 4**

(A) FBXO32 does not ubiquitinate endophilin-1. Analysis of *in vivo* ubiquitination: EGFP-endophilin-1 was co-expressed with HA-ubiquitin in the presence or absence of FBXO32-mCherry. HeLa cell extracts were subjected to immunoprecipitation with anti-GFP antibody and protein ubiquitination was detected by anti-HA Western blotting. Experiment was repeated 3 times (the same result was obtained each time).

(B) FBXO32 does not ubiquitinate endophilin-2. Analysis of *in vivo* ubiquitination: EGFP-endophilin-2 was co-expressed with HA-ubiquitin in the presence or absence of co-expressed FBXO32-mCherry. HeLa cell extracts were subjected to immunoprecipitation with anti-GFP antibody and protein ubiquitination was detected by anti-HA Western blotting. Experiment was repeated 2 times (the same result was obtained each time).

(C) Overall increase in K48-linked (proteasome targeting) ubiquitination in endophilin TKO brains, determined by Western blotting. Right: Quantification from 5 samples/genotype. *$p<0.01$, Student's t test, error bars: SEM.

(D) No change in K63-linked (proteasome-unrelated) ubiquitination in endophilin TKO brains, as determined by Western blotting. Right: Quantification from 5 samples/genotype. $p>0.05$, Student's t test, error bars: SEM.

(E) Endophilin-3 interacts with FBXO32. Representative Western blots from 3 independent experiments of anti-GFP immunoprecipitation from HeLa cell lysate probed with anti-RFP antibody.

(F) GST pull-down from mouse brain lysates using the SH3 domains of endophilin 1, 2 and 3 as baits. Note FBXO32 stronger binding to endophilin-1 and 3 SH3's domains (when films were overexposed, weak band in endophilin-2 SH3 domain sample could also be detected). The experiment was repeated twice.

Figure S4, related to Figure 5

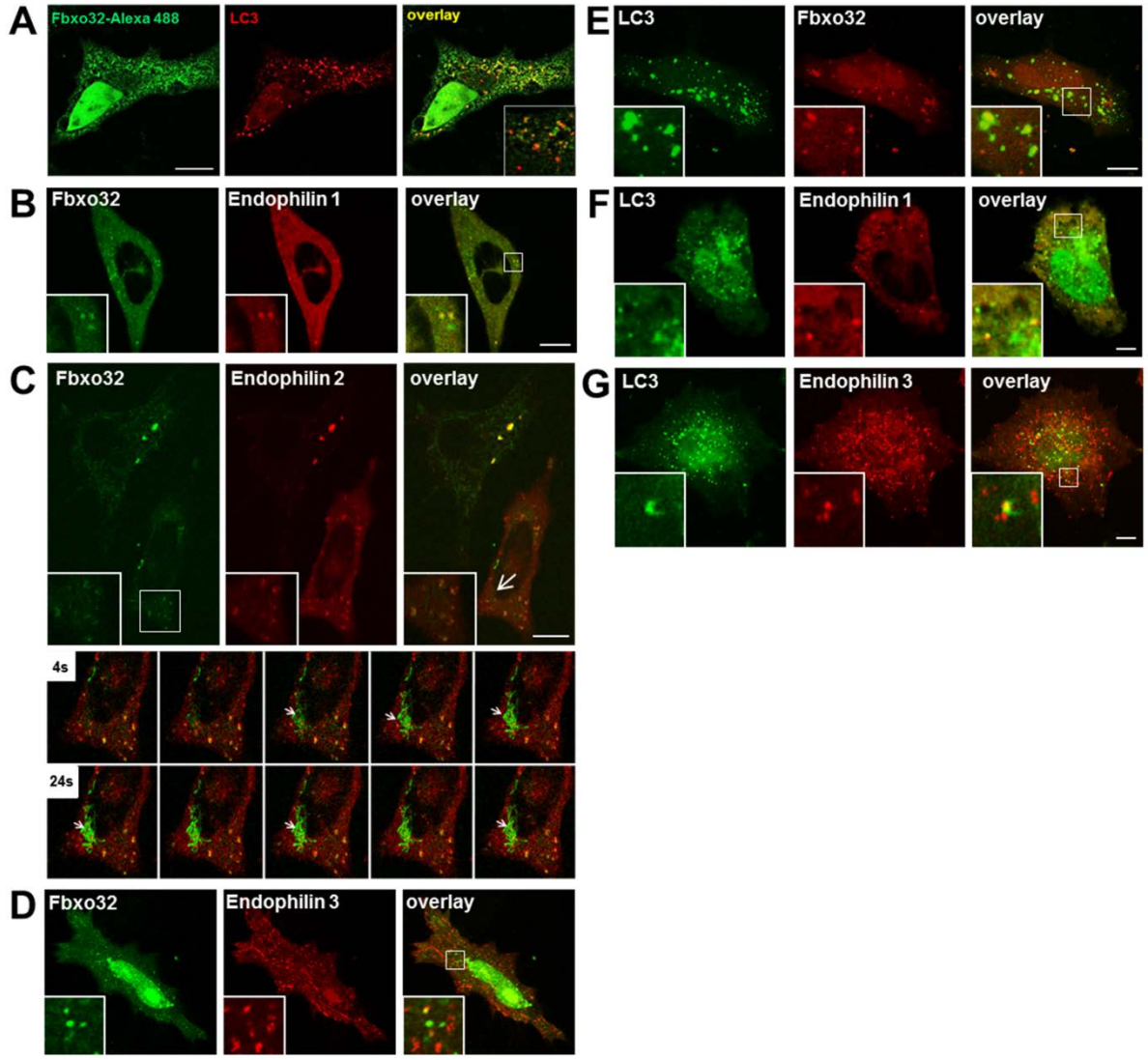

Figure S4. FBXO32 tubulates membranes and co-localizes with clathrin-coated structures and LC3-labelled autophagosomes, related to Figure 5

(A) Native FBXO32 distribution (as detected by immunostaining against FBXO32) in cultured HeLa cell is similar to distribution of overexpressed FBXO32: FBXO32 immunofluorescence was detected in the nucleus and cytosol, and it co-localized partially with autophagosomal maker LC3 (magnified in the inset). Scale bar: 5 µm.

(B) FBXO32-EGFP colocalizes transiently with endophilin-1-mRFP. HeLa cell expressing FBXO32-EGFP (left) and endophilin-1-mRFP (middle); magnified in the inset. Note FBXO32's distribution in the presence of endophilin-1: FBXO32 is mainly extra-nuclear and cytosolic. Scale bar 5 µm.

(C) FBXO32-EGFP colocalizes partially with endophilin-2-RFP (magnified in the inset). A representative MEF with overexpressed FBXO32-EGFP (left) and endophilin-2-mRFP (middle) imaged by spinning-disk confocal microscopy. Scale bar: 5 µm. Below: Image gallery from live time-lapse spinning-disk microscopy from the area indicated by arrow depicting potent tubulation and recruitment of FBXO32 to the tubulating membranes.

(D) FBXO32-mCherry colocalizes transiently with endophilin-3-EGFP. HeLa expressing FBXO32 (left) and endophilin-3 (middle); magnified in the inset. Same magnification is in (A). Images (A-D) were acquired by spinning-disk microscopy.

(E) HeLa cell expressing LC3-EGFP (left) and FBXO32-mCherry (middle) for 26h; starved for 2-3h. Scale bar 5 µm.

(F) Endophilin-A1 showed sparse colocalization with LC3, implying a transient association of endophilin-A1 with autophagosomes. HeLa cells expressing LC3-EGFP (left) and endophilin-A1 protein (middle) were imaged by spinning-disk confocal microscopy after being starved for 2-3h; image on the right shows the overlay. Scale bar 3 µm.

(G) Endophilin-A2 showed sparse colocalization with LC3, implying a transient association of endophilin-A1 with autophagosomes. HeLa cells expressing LC3-EGFP (left) and endophilin-A2 protein (middle) were imaged by spinning-disk confocal microscopy after being starved for 2-3h; image on the right shows the overlay. Scale bar 3 µm.

Figure S5, related to Figure 6

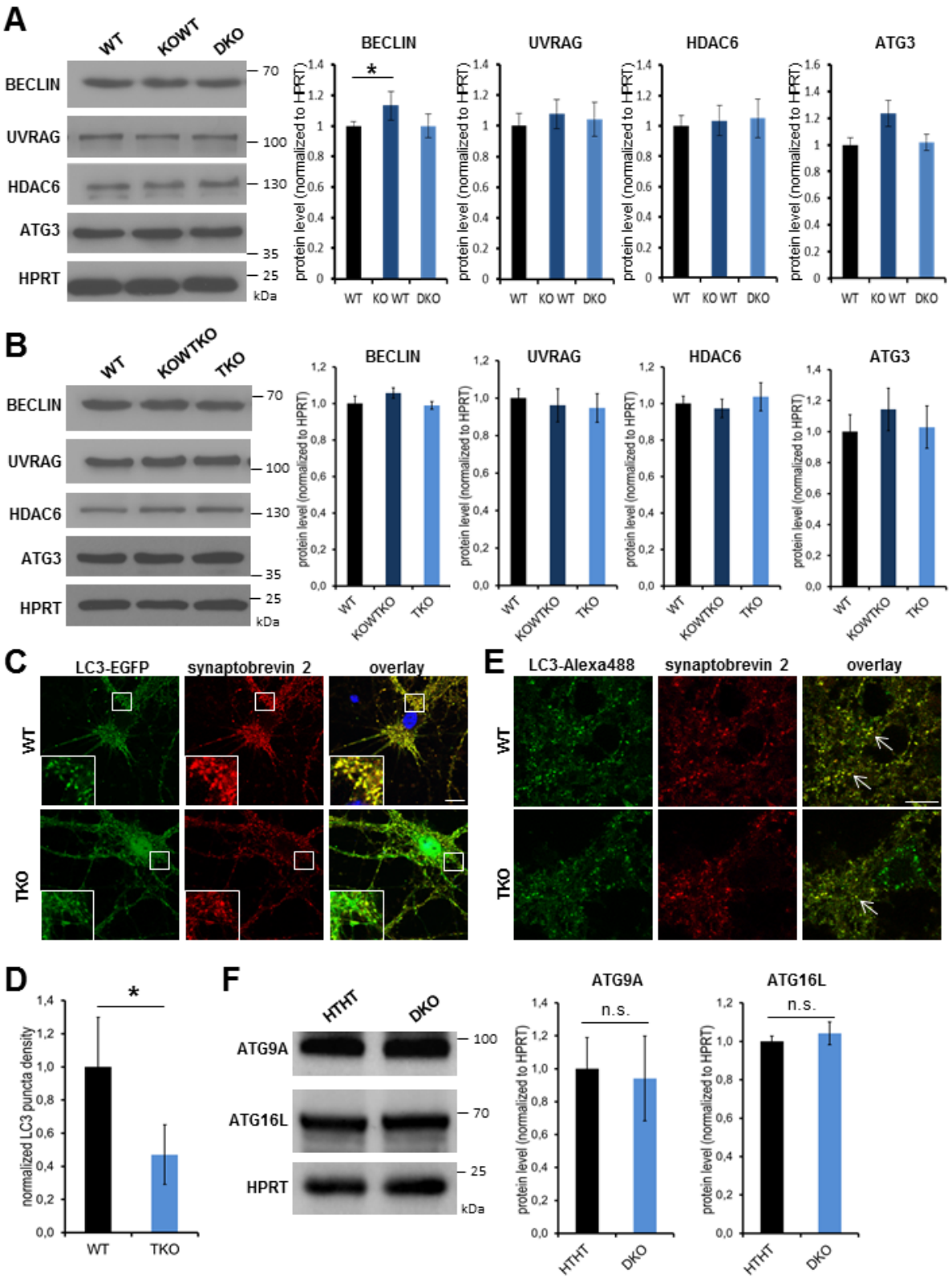

Figure S5. No change in proteins necessary for autophagosome formation or signaling that represses autophagosome formation in endophilin TKO and 1,2 brains, related to Figure 6

(A) Protein analysis by Western blotting revealed no changes in the levels of autophagosomal proteins BECLIN, UVRAG, HDAC6 and ATG3 in endophilin DKO cortex. Right: Histograms showing quantification of the immunoblotting, normalized to the loading control HPRT (at least 6 samples/genotype). $p>0.05$, Student's t test, error bars: SEM.

(B) Protein analysis by Western blotting revealed no changes in the levels of autophagosomal proteins BECLIN, UVRAG, HDAC6 and ATG3 in endophilin TKO whole brain extracts. Right: Histograms showing quantification of the immunoblotting, normalized to the loading control HPRT (at least 8 samples/genotype). $p>0.05$, Student's t test, error bars: SEM.

(C) Autophagosomal marker LC3 revealed less prominent accumulation of LC3 at the synapses of primary endophilin TKO hippocampal neurons. Neurons were treated with 250 nM Torin-1 for 4 hours in the EBSS buffer to accumulate autophagosomes. Note that LC3-signal in WT neuronal processes is a bit more punctate than in TKO neuronal processes, and that WT neurons show better overlap (yellowish signal in the WT overlay, greenish in the TKO overlay) between LC3 and synaptic maker synaptobrevin-2. Scale bar: 5µm.

(D) Decreased LC3 (autophagosome) signal in the endophilin TKO hippocampal cultures: y-axis represents the density of LC3 fluorescence puncta normalized to controls. Three independent experiments were performed and at least 16 images per condition were analyzed. $*p<0.05$, Student's t test; error bars: SEM.

(E) Immunostaining for LC3 (autophagosomal marker) and synaptobrevin-2 (synaptic marker) in primary neurons prepared from WT and endophilin TKO hippocampi. Neurons were treated as described above. There is less prominent accumulation of LC3-signal at the synapses in endophilin TKO neurons. LC3-positive autophasomal structures in the cell body (blue arrow) seem less affected than LC3-positive autophagosomal structures at the synapses (white arrow) in endophilin TKO neurons. Scale bar: 5µm.

(F) Protein analysis by Western blotting revealed no changes in the levels of autophagosomal proteins ATG9A and ATG16L in endophilin 1,2 DKO cortexes. Right: Histograms showing quantification of the immunoblotting, normalized to the loading control HPRT (at least 4 samples/genotype). $p>0.05$, Student's t test, error bars: SEM.

Figure S6, related to Figure 7

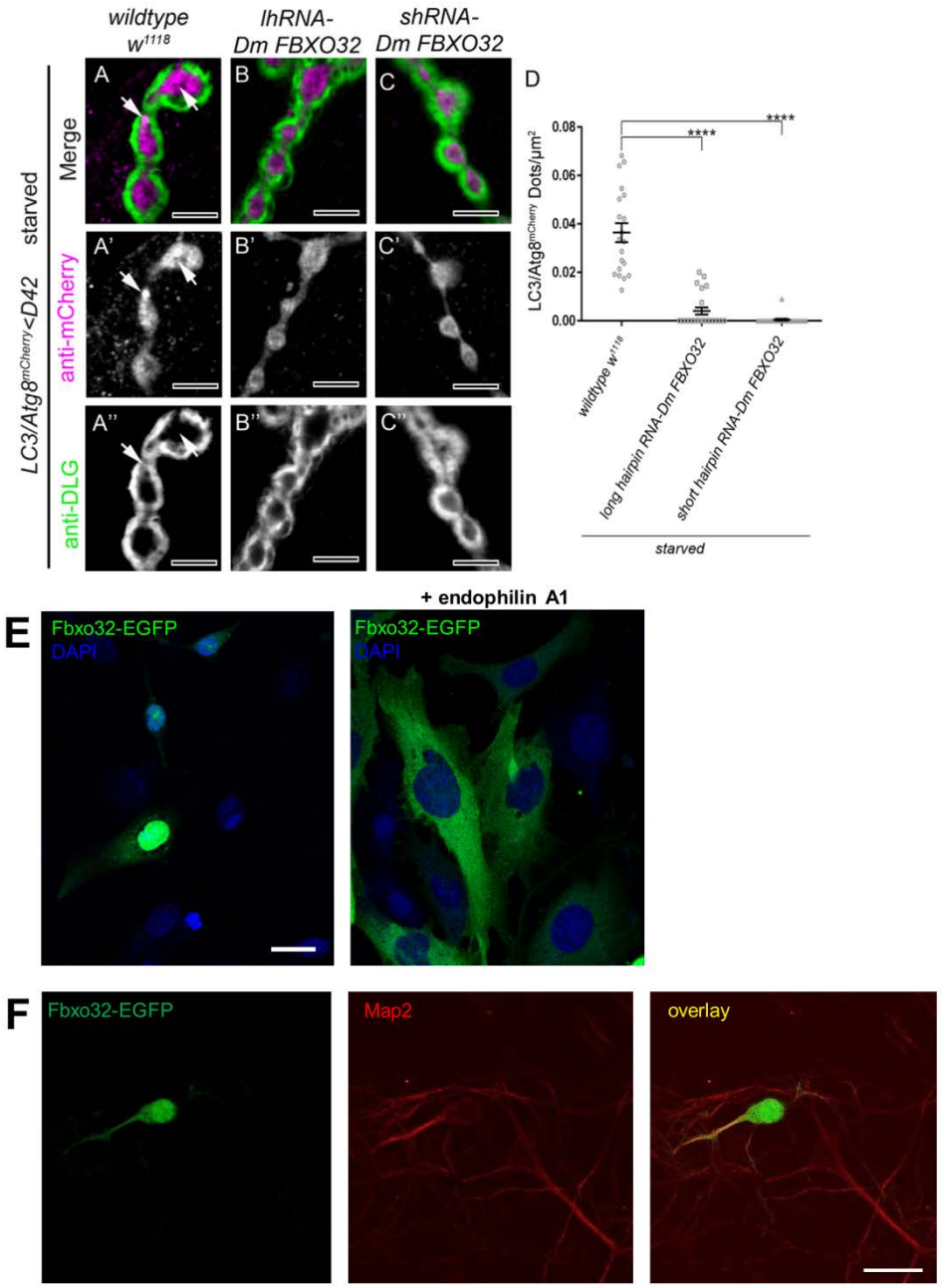

Figure S6. FBXO32 is required for autophagy at drosophila NMJ and its upregulation causes apoptosis in cultured primary neuronal cells, related to Figure 7.

(A-C'') Confocal imaging of 4 h-starved neuromuscular junction boutons (NMJ) of WT control animals (A-A''), animals expressing long hairpin RNAi against Drosophila FBXO32 (B-B'') and animals expressing short hairpin RNAi against Drosophila FBXO32 (C-C'') co-expressing ATG8-mCherry under control of the D42-Gal4 driver to drive expression in the motor neurons and NMJ. (A-C) Shows merged images of anti-mCherry (magenta, A'-C') to mark autophagosomes (arrows in A-A') and anti-DLG (green, A''-C'') to label the post synaptic site.

(D) Quantification of the number of ATG8-mCherry dots per bouton area (arrows) and statistical analysis using 1-way ANOVA followed by Post Hoc Mann-Whitney test ****$p<0.0001$, $n>21$. Individual data points are shown and the mean±SD is indicated. Scale bars: 5 µm

(E) Representative images of fixed HeLa cells co-transfected with FBXO32-EGFP and mRFP (left) and FBXO32-EGFP and endophilin-1-mRFP (right) for 30h, co-stained with DAPI. mRFP and endophilin-1-mRFP signals are not shown to emphasize the difference in FBXO32 distribution. Gain was kept constant for all images. Note that less than 50% of FBXO32-transfected cells survive on average (left image). Scale bar: 7 µm.

(F) Primary hippocampal neurons transfected with FBXO32-EGFP under chicken-β-actin promoter. Neurons were transfected on DIV0 by electroporation, fixed on DIV14, co-stained for MAP2 and imaged by confocal microscopy. Less than 15% FBXO32-transfected neurons are detected at DIV14 (when compared to EGFP-expressing neurons). The surviving FBXO32-transfected neurons did not appear healthy and had only few short processes. Scale bar: 7 µm.

Supplemental Movies

Movie S1. Endophilin 1,2 DKO and littermate 1KO-2WT mice, related to Figure 1. Mice have a 129Sv/J background (all our endophilin lines, including 1,2 DKO, were also backcrossed to C56BL/6J for 5 generations). Endophilin 1,2 DKO mouse displays ataxia (staggering, lack of balance, loss of muscle control, slow eye movement, etc.), littermate 1KO-2WT mouse does not have obvious movement deficits.

Movie S2. Endophilin 1KO-2WT-3KO and endophilin 1KO-2HT-3KO mice running in a DigiGait treadmill at 20 cm/s, related to Figure 1. Left: endophilin 1KO-2WT-3KO, right endophilin 1KO-2HT-3KO. Top: video, bottom: extracted paw signal by DigiGait analysis software. Note that endophilin 1KO-2HT-3KO mice have an altered walking pattern (real-time video rate has been slowed down 3x).

Movie S3. FBXO32-EGFP expressed in MEF for 22h and imaged by spinning-disc confocal microscopy, related to Figure 5. This movie shows distribution of FBXO32 in MEF: FBXO32 is predominantly cytosolic, although it often accumulated in the nucleus; it is enriched at dynamic organelle-like structures exemplifying its role in trafficking. Time-lapse images were captured every 4s, video runs at 10 frames/s.

Movie S4. FBXO32-EGFP and LC3-mRFP expressed in HeLa for 28h and imaged by spinning-disc confocal microscopy, related to Figure 5. The movie shows FBXO32 (green) association with LC3-positive autophagosomes (red). Time-lapse images were captured every 4s, video runs at 10 frames/s.

Movie S5. FBXO32-EGFP and endophilin-2-mRFP expressed in MEF for 21h, related to Figure 5. Imaged by spinning-disc confocal microscopy. Note that FBXO32 (green) and endophilin (red) co-localized on trafficking organelles and tubular structures. **Inset** shows a zoomed image with dynamic tubule labelled with both FBXO32-EGFP and endophilin-2-mRFP. Time-lapse images were captured every 4s, video runs at 10 frames/s.

Movie S6. Magnified view of HeLa expressing FBXO32-EGFP (green), LC3-mRFP (red) and endophilin-2-iRFP (magenta) for 22h, related to Figure 5. Imaged by spinning-disc confocal microscopy. Size of inset 3 μm. Time-lapse images were captured every 4s, video runs at 10 frames/s

Movie S7. Magnified view of hippocampal neuron expressing endophilin-2-EGFP (green) and ATG5-mCherry (red), related to Figure 5. Imaged by spinning-disc confocal microscopy. Size of inset 4 μm. Time-lapse images were captured every 4s, video runs at 10 frames/s.

Tables

Table 1-7: See attached Excel file

Table 1. RNA sequencing of endophilin TKO and endophilin 1,2 DKO samples, related to Figure 2. Genotype, total reads and mapped reads are shown for each sample.

Table 2. Comparison of endophilin TKO and littermate 1KO-2WT-3KO samples, related to Figure 2. The ENSEMBL gene identifier is the key identifier for each gene. Shown for each gene, from left to right, are the corresponding gene symbol, description, genomic coordinates (including chromosome, with start and end positions), average reads across all samples, average reads across KOWTKO samples, average reads across TKO samples, logarithm (base 2) of the fold change between the average TKO reads and the average KOWTKO reads, nominal p-value and adjusted p-value.

Table 3. Comparison of endophilin TKO and WT samples, related to Figure 2. The ENSEMBL gene identifier is the key identifier for each gene. Shown, from left to right are the corresponding gene name, description, genomic coordinates (including chromosome, with start and end positions), average reads across all samples, average reads across WT samples, average reads across TKO samples, logarithm (base 2) of the fold change between the average TKO reads and the average WT reads, nominal p-value and adjusted p-value.

Table 4. Crossing of TKO and 1,2 DKO differentially-expressed genes with gene lists of ataxia and Parkinson's disease, related to Figure 2. For each comparison between endophilin mutants and controls (1,2DKOxWT, 1,2DKOx1KO-2WT, TKOxWT, TKOx1KO-2WT-3KO), the threshold for differential expression was an adjusted p-value<0.01 and a $\log_2$FC>0.4. The genes that met those criteria were considered differentially-expressed genes (DEGs) for each comparison, and the number of genes is shown in the second column next to each comparison. The number of DEGs in each comparison that is also included in the ataxia and Parkinson's disease (PD) lists, the corresponding enrichment score and p-value are shown. The last columns indicate the symbols of the genes that are present in the DEG lists and also ataxia and PD for each comparison.

Table 5. Comparison of endophilin 1,2 DKO and 1KO-2WT samples, related to Figure 2. The ENSEMBL gene identifier is the key identifier for each gene. Also shown, from left to right are the corresponding gene name, description, genomic coordinates (including chromosome, with start and end positions), average reads across all samples, average reads across 1KO-2WT samples, average reads across 1,2 DKO samples, logarithm (base 2) of the fold change between the average 1,2 DKO reads and the average 1KO-2WT reads, nominal p-value and adjusted p-value.

Table 6. Comparison of endophilin 1,2 DKO and WT samples, related to Figure 2. The ENSEMBL gene identifier is the key identifier for each gene. Shown, from left to right are the corresponding gene name, description, genomic coordinates (including chromosome, with start and end positions), average reads across all samples, average reads across WT samples, average reads across 1,2 DKO samples, logarithm (base 2) of the fold change between the average 1,2 DKO reads and the average WT reads, nominal p-value and adjusted p-value.

Table 7. List of DEGs when endophilin TKO samples are compared against all controls pooled together, related to Figure 2. The threshold for differential expression was set at nominal p-value<0.01 to generate a gene list with optimal size for the pathway analysis algorithm (IPA software). For each gene, the ENSEMBL identifier and the fold change are presented.

Table 8. Upstream regulators of TKO transcriptome, related to Figure 2. These regulators were identified by Ingenuity Pathway Analysis, under the criteria of a p-value<0,05. To limit false positives, the analysis was restricted to the regulators that were present in the list of differentially expressed genes. The logarithm of the fold change for each regulator in the TKO dataset is presented.

Supplemental Experimental Procedures

Cell morphology assessment

Golgi staining was performed with the FD Rapid GolgiStain™ Kit (FD Neurotechnologies Inc.) following the manufacturer's instructions. In short, animals were euthanized and the whole brain dissected, rinsed and immersed in the impregnation solution for 14 days. After 3 days incubation in solution C, brains were quickly frozen in isopentene using liquid nitrogen. Immediately after freezing, the brains were cut using a cryostat (Leica CM1859 UV) at 100 or 150 µm thickness and stained the next day. For staining, slides were incubated in working solution for 10 min and dehydrated before being embedded in Permount® (Entellan New, Merck). Samples were imaged on a Nikon AZ100 microscope.

RNA-sequencing

RNA for RNA-sequencing experiments was isolated using Tri-Reagent (Sigma) according to the manufacturer's instructions. RNA-seq libraries were prepared using the TruSeq® RNA Sample Preparation v2 kit and the TruSeq® Small RNA Preparation kit from Illumina. The library quality was checked using an Agilent 2100 Bioanalyzer and a Qubit dsDNA HS Assay Kit. The sample concentration was measured using a Qubit dsDNA HS Assay Kit and adjusted to 2 nM before sequencing (50 bp single end) on a HiSeq 2000 (Illumina) using TruSeq SR Cluster Kit v3-cBot-HS and TruSeq SBS Kit v3-HS according to the manufacturer's instructions. At least 7 biological replicates per condition were used for sequencing.

Read alignment and quality assessment: Murine RNA-seq data was aligned to the *Mus musculus* mm10 genome using STAR aligner (Version 2.3.0e_r291) with default options and generating alignment files in BAM format (Dobin et al., 2013). Read counts for all genes and all exons (Ensembl annotation v72) were obtained using FeaturesCount (version 1.4.6) (Liao et al., 2014). RNA-seq data was subjected to an in-house quality control workflow (Capece et al., 2015; Halder et al., 2016). During the quality assessment sequencing data was analyzed for the percentage of aligned, uniquely aligned and unaligned reads to determine possible sequencing biases, while sequencing depth was determined by the average per base coverage for each sample (Suppl. Table 1). Principal component analysis (PCA) was performed on RNA-seq expression values as previously described (Capece et al., 2015). One sample that did not meet quality standards was removed from further analysis.

Differential expression and pathway analysis: Read counts, as generated in the 'Read alignment and quality assessment' section, were used to find differentially expressed genes (DEGs) between the aforementioned mutant and control samples using DESeq2 (Love et al., 2014). Genes with an adjusted p-value smaller than 0.01 and an absolute $\log_2$ fold change (logFC) higher than 0.4 were considered to be DEGs. Results of the differential expression analysis can be found in Supp Table 1-3 and 5-6. For functional enrichment analyses we used Webgestalt and only considered categories significant with an adjusted p-value < 0.05. Genes with a nominal p-value smaller than p=0.01 were considered to be DEGs for input into Ingenuity Pathways Analysis (IPA). In multiple instances, perturbation of the genomic surroundings of knocked-out genes have been reported (Chandrasekharan et al, 2010; Rampon et al, 2008; Yang et al, 2007; Wang et al, 2014). After mapping the sequence reads to the transcriptome, we blocked the regions within 1 million base pairs of the genes knocked-out (endophilins 1, 2, 3), to ensure that genes whose expression may be affected by the perturbation of promoters or enhancers nearby are not skewing the pathway analysis.

Quantitative RT-PCR

RNA extraction and purification were performed using via Qiagen or Macherey-Nagel RNA extraction kits according to manufacturer's instructions. RNA quantification and quality control were done using Nanodrop (PeqLab), and cDNA was synthesized with High-Capacity cDNA Reverse Transcription Kit (Applied Biosystems) according to the manufacturer's instructions. cDNA was diluted 1:100, and each 8 µl reaction contained 4 µl diluted cDNA, 0,2 µl dilutions of each primer (from 25 µM stock) and 3,6 µl iTaq Universal SYBR Green Supermix (Bio-Rad).

Biochemical procedures

Brains or dissected brain samples were stored at -80°C long-term, and shortly before use were placed in -20°C blocks until being quickly added to tubes containing three 5mm metallic beads and 1080 µL of homogenization buffer [20mM HEPES pH 7.4, 150mM NaCl, 1mM EDTA, 1mM DTT, Complete Protease Inhibitor (Roche) and phosSTOP phosphatase inhibitor (Roche)] immediately prior to tissue homogenation. Samples were oscillated vigorously on the bead mill apparatus (Retsch MM400) for 1 minute at 20 Hz (p0 animals) or 30 Hz (1,2 DKO p14-21 and old animals). Samples were subjected to a 10s quick-spin and 120 µL of 20% sodium dodecyl sulfate (SDS) was added to completely solvate the high proportion of lipids and cholesterol in brain tissue. Samples were again subjected to 1 minute oscillation on the bead mill at 20 Hz for p0, and 30 Hz for young and old animals. A quick-spin again reduced the foam and bubbles. If any visible opaque streaks or solid matter remained at this point, the above two steps were repeated 1-2x. 18-20 month-old animals required 5 minutes of total homogenization and addition of greater volume to solvate the tissue – 2 additional 1-minute homogenizations after the 4th 1 minute homogenization step, an additional 300 uL of pre-mixed SDS and homogenization buffer (30 µL 20% SDS and 270 µL homogenization buffer) were added to solvate the remaining clumps of lipid and tissue. This volume was sufficient to homogenize the remaining solid matter for a final volume of 1500 µL in the old animals. The final homogenate was then subjected to vigorous mixing (15–30x) with a 27-gauge needle and 1 mL syringe to break up any semisolid remnants and shear viscous DNA strands so that the mixture was fluid and homogeneous for use in SDS-PAGE gels.

Samples were then quantitated with Pierce BCA (Thermo Scientific) in a 40x dilution to fall in the linear range as determined by the BSA standard curve using the BSA aliquot provided in the BCA kit. 3 µL of sample were diluted in 117 µL of dH_2O to give 120 µL of diluted sample, then 50 µL of diluted sample was added to 1 mL of the 1:50 BCA working solution. This last step was done in duplicate for each sample. These mixes were prepared in glass test tubes and incubated in a 37°C water bath for 30 minutes, then transferred to plastic cuvettes and read on a spectrophotometer (Eppendorf).

The SDS-PAGE gels were prepared at 1 mm thickness in 4% stacking and 12% resolving concentrations. For every multiple of 4 gels, the stacking component was prepared with 6.43 mL dH_2O, 2.5 mL 0.5M Tris-HCl pH 6.7, 100 µL 10% SDS, 1 mL 40% acrylamide-bis-acrylamide 30:1, 100 µL ammonium persulfate and 20 µL TEMED, and the resolving component was prepared with 8.7 mL dH_2O, 5 mL 1.5M Tris-HCl pH 8.7, 200 uL 10% SDS, 6 mL 40% acrylamide-bis-acrylamide 30:1, 200 uL ammonium persulfate and 20 uL TEMED. Gels were loaded with 50 ug of protein per well in volumes of 20 µL of diluted sample and 4 µL of 6x loading buffer (10 mL: 1.2 g sodium dodecyl sulfate, 4.7 mL glycerol, 1.2 mL 0.5M Tris pH 6.8, 0.93 g dithiothreitol, 6 mg bromophenol blue, 2.1 mL dH_2O). Samples were always diluted to a final concentration of 50 µg using

additional sample buffer. Wells with no sample were filled with the corresponding buffer and loading buffer in the same proportion as for sample-containing wells (20 µL sample/buffer plus 4 µL loading buffer per well). Protein ladder was PageRuler Prestained Plus (Thermo Scientific).

Immunoprecipitation experiments: For Trap®-GFP immunoprecipitation, Hela cells ($1.2x10^6$) were plated in a 10cm plate and transfected with Lipofectamine 3000 after 3-4 hours. Endophilin-1, 2 or 3 tagged with EGFP were co-expressed either with FBXO32-mCherry or mCherry control (6.5µg/plate in total). The cells were harvested 30 hours after transfection and lysed. We used Chromotek Trap®-GFP agarose beads (Chromotek, Germany) and followed manufacturer's protocol. The eluate was loaded onto SDS-PAGE gel followed by an immunoblot analysis for Cherry (RFP antibody 5F8, Chromtek, Germany) using standard protocol. Three independent experiments were performed.

Pull-down experiments: Pull-down experiments with GST-endophilin-1-SH3, GST-endophilin-2-SH3and GST-endophilin-3-SH3 domains were performed as previously described (Cao et al, 2014). The same method was used for GST-FBXO32 pull-down experiments. Three independent experiments were performed.

Autophagy in primary neurons and clonal cells

For autophagy-related experiments, we electroporated dissociated neurons in suspension (P3 Primary Cell 4D-Nucleofector® X Kit L, Amaxa, Lonza) before plating. If electroporation is used, it is essential that promoter is mild - all constructs used in neurons had chicken β-actin or synapsin promoter. For primary neuronal cell transfection, we followed manufacturer's instructions (Lonza). On average, transfection efficiency of ~60% and ~70% neuronal survival was achieved (protocol CA138 and CL133, Nucleofactor-II). We used transfected neurons 12-16 days after transfection/plating (only strong, good-looking neuronal preparations where cell bodies and large processes were "shiny" and no cell inclusions/vacuoles or distressed cells were visible). Further, the osmolarity of neuronal medium was measured before experiment: osmolarity of buffers/solutions that were subsequently used was adjusted to match medium in which neurons grew. Buffers/solutions were warmed up to 37°C before use, and incubation with drugs was done in the incubator (37°C, 5% CO_2 in a humidified atmosphere). We used 250nM Torin-1 (BioVision) in the EBSS buffer (Gibco) without B27 supplement (Gibco) for 4 h to induce autophagy. Neurons were subsequently imaged by spinning-disk microscopy (Perkin Elmer Ultraview spinning-disk setup that consists of Nikon Ti-E Eclipse inverted microscope equipped with Perfect Focus, 60x CFI Plan Apo VC Nikon objective and 14 bit electron-multiplied CCD camera/Hamamatsu C9100), or fixed with 3,7% paraformaldehyde and 1% sucrose in the Tyrode buffer for 1h, immunostained for synaptic markers (e.g. synaptobrevin-2) and imaged by confocal microscopy (a LSM 710 setup by Zeiss). In neurons without autophagy induction, mildly expressed LC3 looked cytosolic with some brighter puncta. Upon autophagy induction, bright puncta were increased in cell periphery (processes) as well as in the cell body.

Endophilin TKO neurons have less synaptobrevin-2 (Milosevic *et al*., 2011), even so, the overlap between LC3 and synaptobrevin-2 was less prominent in endophilin TKO neurons.

Clonal cells (MEF, Hela) that mildly express fluorescently labelled-LC3 in addition to other probes (e.g. FBXO32, endophilins) were starved for at least 2 hours before being imaged by spinning-disk microscopy (the same setup as detailed above was used).

Colocalization analysis

Given that the majority of respective fluorescent signals were cytosolic, colocalization was evaluated semi-automatically using object-based overlap analysis and ImageJ JACoP plugin (Bolte and Cordelieres, 2006). In short, the image was first segmented into objects and background (i.e. bright fluorescent objects are segmented from the image) and then their spatial relationship (overlap) was measured. The same analysis was performed with flipped images and random colocalization was subtracted for every image.

The results were verified by complementary manual colocalization analysis based on morphological criteria. We used a procedure similar to one previously described (Lang et al, 2002). Namely, circles were superimposed on bright fluorescent spots in the FBXO32 (or LC3) channel and transferred to identical image locations in the endophilin channel. If the fluorescence intensity maximum in the endiophilin channel was located in the same quadrant of the circle and the morphology of the signal resembled that of the FBXO32 signal, the circle was rated as positive (colocalized). If not, the circle was rated as negative (not colocalized). Clusters for which a clear assignment was not possible were considered as neutral and excluded from further analysis. To be able to correct for random background colocalization, the circles were also transferred to a mirror image of the endophilin channel. Corrections were made to ensure that circles on the mirrored image were also placed within the cell. Both methods have yielded similar results.

Plasmids

The pCMV-SPORT6-FBXO32 plasmid was purchased from Thermo Scientific. The FBXO32-EGFP construct was generated by inserting mouse FBXO32 into pEGFP-N1 (Clonetech) using EcoRI and AgeI restriction sites. The pCherry-N1 plasmid was generated by replacing EGFP in pEGFP-N1 vector with mCherry (as published in Milosevic *et al*, 2011). The FBXO32-mCherry construct was generated by inserting mouse FBXO32 into pCherry-N1 using SalI and BamHI restriction sites. The pCAG-FBXO32-EGFP plasmid was generated by amplifying mouse FBXO32 and inserting it into pCAG-EGFP (Milosevic et al, 2011) using SalI and BamHI restriction sites. The pGEX-6P-1-FBXO32 plasmid was generated by inserting mouse FBXO32 using BamHI and EcoRI sites. A pCAG-EGFP-LC3 plasmid was generated by amplifying rat LC3 and inserting it into pCAG-EGFP (Milosevic et al, 2011) using BglII and SalI restriction sites. The endophilin A2-mRFP and endophilin A3-mRFP construct was generated by amplifying rat endophilin A2 and human endophilin A3 respectively and inserted them into pcDNA3.1-mRFP using BamHI and HindIII. All constructs have been verified by sequencing and restriction enzyme digestions. The constructs with the CAG promoter were verified in cultured fibroblasts before their use in neurons.

The pEGFP-LC3, pmRFP-LC3 and pGFP-Ub-G76V were purchased from Addgene. The pCAG-EGFP-N1 (Milosevic et al, 2011), pcDNA3.1-HA-Ubiquitin (rat; Cao *et al*, 2014), pEndophilinA1-mRFP (Perera et al, 2006), pmRFP-clathrin LC (Perera et al, 2006) were a gift from P. De Camilli (Yale University, New Haven, CT, USA)

Caspase activity assay

Caspase 3/7 apoptosis assay was performed with the ApoTox-Glo™ Triplex Assay (Promega) kit according to a modified version of the manufacturer's protocol for 96 well plates. Cells were seeded (~10000 cells/well) in

luminescence-compatible plates 24h before. Prior to the assay, cells were treated with 0.4M sorbitol for 1 hour to induce osmotic cell death, while others were left untreated to assess basal apoptotic levels. The cells were washed, and 40µl/well medium was added, including empty wells for blank reaction assessment. 10 µL/well Caspase 3/7 mixed reagent was added, incubated at RT in the dark on a rotational shaker. Untreated wells for each condition were reserved for protein quantification by the BCA protocol (Pierce). These cells were lysed with 75 µL/well of 1,5% n-dodecylmaltoside in PBS for 1 hour on an orbital shaker. Then, 59 µL dH_2O and 100 µL 1:25 BCA working solution were added, mixed and incubated for 30 min at 37°C. Samples were read on a Synergy H1 plate reader (Biotek) at 561 nm and normalized to a standard curve. Data were then normalized to the protein content for each condition.

Experimental work with Drosophila

Fly Stocks and genetics: Flies were grown on standard cornmeal and molasses medium at 25°C. The following Drosophila stocks were from the Bloomington Stock Center: w[*]; P{w[+mW.hs]=GawB}D42, y1 v1; P{TRiP.JF01340}attP2, y1 sc* v1; P{TRiP.HMS02671}attP4. P[w{+}UAS-Atg8-mCherry was obtained from T. Neufeld.

Immunohistochemistry and induction of autophagy: To induce autophagy, we either used starvation or stimulation. For starvation, early third instar larvae were placed on petri dishes containing 20% sucrose and 1% agarose for 4 h prior to experimentation 2. Immunohistochemistry of third instar larval NMJs was performed by dissecting larvae in HL3 on sylgard plates and then fixing with paraformaldehyde 4% in HL3 for 20 min. After 45 min permeabilization with 0.4% Triton X-100 in PBS larvae of different genotypes were physically marked and treated in the same tube for the labeling. Samples were preblocked with 10% NGS-PBT (0.1% Triton X-100 and 0.4% Triton X-100 in PBS, respectively) for 30-60 min and then incubated with primary antibodies over-night at 4°C. Samples were washed several times and then incubated with secondary antibodies in PBT with 10% NGS for 2 h at room temperature. The samples were finally mounted in Vectashield (Vector Laboratories).

Imaging and Antibodies: Fixed samples were imaged on a Nikon A1R confocal microscope through a 60X NA1.2 water immersion lens. Single confocal planes of boutons were scanned using identical settings. Fluorescence was quantified using NIH ImageJ: Average pixel intensities in boutonic areas were calculated or the number of mCherry-positive autophagosomes was measured using particle analysis of a binary image. The number of mCherry-positive autophagosomes was measured using particle analysis of a binary image by first applying a threshold mask and a selection of boutonic areas in a single plane of mCherry positive synapses.

Statistical analysis: Statistical significance was determined using GraphPad Prism software, Version 6 (Graphpad, San Diego, CA, USA. www.graphpad.com). Parametric data were analyzed with one-way analysis of variance tests (ANOVA), followed by Tukey-Kramer testing. Non-parametric data was analyzed using Kruskal-Wallis followed by Dunn's test. Significance of statistical difference was defined as ****$p<0.0001$, ***$p<0.001$, **$p<0.01$,*$p<0.05$, ns $p>0.05$.

Antibodies used for Western blotting

FOXO3a (Cell Signaling, rabbit, 75D8), 1:1000

P-FOXO3a (Cell Signaling, rabbit, Ser253), 1:1000

FOXO1 (Cell Signaling, rabbit), 1:1000

FBXO32 (Novus, goat), 1:1000

FBXO32 (ECM, rabbit, AX2045), 1:1000

ATG5 (Cell Signaling, rabbit) 1:1000

ATG9A (abcam, rabbit), 1:1000

ATG16L1 (MBL, rabbit), 1:1000

LC3B (Cell Signaling, rabbit, D11), 1:1000

ATG3 (Cell Signaling, rabbit, #3415), 1:1000

BECLIN1 (Cell Signaling, mouse) 1:500

HDAC6 (Millipore, rabbit, 07-732) 1:1000

UVRAG (Sigma Aldrich, rabbit, HPA016932) 1:1000

CDK5 (Santa Cruz, rabbit) 1:2000

GSK3B (Cell Signaling, rabbit) 1:8000

P-GSK3B (Cell Signaling, rabbit) 1:1000

HPRT (Abcam, rabbit) 1:1000

Ubiquitin (mouse FK2) 1:2000

Endophilin 1 (gift of P. De Camilli and SySy, both rabbit) 1:1000

Endophilin 2 (gift of P. De Camilli, rabbit) 1:1000

Antibodies used for immunolabelling

P-FOXO3a (Cell Signaling, rabbit, Ser253) 1:200

FBXO32 (Novus, goat), 1:200

LC3B (Cell Signaling, rabbit, D11) 1:1000

Synaptobrevin2 (SySy, mouse, 69.1) 1:500

GFAP (SySy, mouse, 64F6) 1:500

mCherry (Novus; chicken, NBP2-25158), 1:1000

DLG (DSHB; mouse, 4F3), 1:500

MAP2 (Chemicon, rabbit), 1:1000

Cleaved caspase-3 (Cell Signaling, rabbit), 1:600

Secondary antibodies used for immunolabelling

Anti-rabbit Alexa Fluor 488 (LifeTechnology, goat), 1:200 and 1:1000 (Drosophila)

Anti-rabbit Alexa Fluor 555 (LifeTechnology, goat), 1:1000

Anti-rabbit Alexa Fluor 594 (LifeTechnology, goat), 1:200

Anti-mouse Alexa Fluor 488 (LifeTechnology, goat), 1:200

Anti-mouse Alexa Fluor 594 (LifeTechnology, goat), 1:200

Anti-mouse Alexa Fluor 647 (Invitrogen) 1:400

Supplemental References

Bolte, S. and Cordelières, F.P. (2006). A guided tour into subcellular colocalization analysis in light microscopy, Journal of Microscopy 224, 3: 213-232.

Cao, M., Milosevic, I., Giovedi, S., and De Camilli, P. (2014). Upregulation of Parkin in endophilin mutant mice. J Neurosci 34, 16544-16549.

Capece, V., Garcia Vizcaino, J.C., Vidal, R., Rahman, R.U., Pena Centeno, T., Shomroni, O., Suberviola, I., Fischer, A., and Bonn, S. (2015). Oasis: online analysis of small RNA deep sequencing data. Bioinformatics 31, 2205-2207.

Chandrasekharan, K., Yoon, J.H., Xu, Y., deVries, S., Camboni, M., Janssen, P.M., Varki, A., and Martin, P.T. (2010). A human-specific deletion in mouse Cmah increases disease severity in the mdx model of Duchenne muscular dystrophy. Science translational medicine 2, 42ra54.

Dobin, A., Davis, C.A., Schlesinger, F., Drenkow, J., Zaleski, C., Jha, S., Batut, P., Chaisson, M., and Gingeras, T.R. (2013). STAR: ultrafast universal RNA-seq aligner. Bioinformatics 29, 15-21.

Lang, T., Margittai, M., Holzler H. and Jahn, R. (2002). SNAREs in native plasma membranes are active and readily form core complexes with endogenous and exogenous SNAREs. J. Cell Biol. 158:751-760

Liao, Y., Smyth, G.K., and Shi, W. (2014). featureCounts: an efficient general purpose program for assigning sequence reads to genomic features. Bioinformatics 30, 923-930.

Love, M.I., Huber, W., and Anders, S. (2014). Moderated estimation of fold change and dispersion for RNA-seq data with DESeq2. Genome Biol 15, 550.

Milosevic, I., Giovedi, S., Lou, X., Raimondi, A., Collesi, C., Shen, H., Paradise, S., O'Toole, E., Ferguson, S., Cremona, O., et al. (2011). Recruitment of endophilin to clathrin-coated pit necks is required for efficient vesicle uncoating after fission. Neuron 72, 587-601.

Perera, R.M., Zoncu, R., Lucast, L., De Camilli, P., and Toomre, D. (2006). Two synaptojanin 1 isoforms are recruited to clathrin-coated pits at different stages. Proceedings of the National Academy of Sciences of the United States of America 103, 19332-19337.

Rampon, C., Bouillot, S., Climescu-Haulica, A., Prandini, M.H., Cand, F., Vandenbrouck, Y., and Huber, P. (2008). Protocadherin 12 deficiency alters morphogenesis and transcriptional profile of the placenta. Physiological genomics 34, 193-204.

Wang, G.X., Zhao, X.Y., Meng, Z.X., Kern, M., Dietrich, A., Chen, Z., Cozacov, Z., Zhou, D., Okunade, A.L., Su, X., et al. (2014). The brown fat-enriched secreted factor Nrg4 preserves metabolic homeostasis through attenuation of hepatic lipogenesis. Nature medicine 20, 1436-1443.

Tian A., Baumgart T. (2009) Sorting of lipids and proteins in membrane curvature gradients. Biophys. J. 96, 2676–2688.

Yang, S., Farias, M., Kapfhamer, D., Tobias, J., Grant, G., Abel, T., and Bucan, M. (2007). Biochemical, molecular and behavioral phenotypes of Rab3A mutations in the mouse. Genes, brain, and behavior 6, 77-96.